Evidence of tunable magnetic coupling in hydrogenated graphene

Shimin Cao [ORCID],[1] Chuanwu Cao [ORCID],[1] Shibing Tian,[2] and Jian-Hao Chen [ORCID][1,3,4,*]

[1]*International Center for Quantum Materials, School of Physics, Peking University, Beijing 100871, China*
[2]*Institute of Physics, Chinese Academy of Sciences, Beijing 100190, China*
[3]*Key Laboratory for the Physics and Chemistry of Nanodevices, Peking University, Beijing 100871, China*
[4]*Beijing Academy of Quantum Information Sciences, Beijing 100193, China*

Many efforts have been devoted to understanding the origin and effects of magnetic moments induced in graphene with carbon atom vacancy, and light adatoms like hydrogen or fluorine. In the meantime, the large negative magnetoresistance (*MR*) widely observed in these systems is not well understood, nor has it been associated with the presence of magnetic moments. In this paper, we study the systematic evolution of the large negative *MR* of *in-situ* hydrogenated graphene in ultrahigh-vacuum (UHV) environment. We find for most combinations of electron density (n_e) and hydrogen density (n_H), *MR* at different temperature can be scaled to $\alpha = \mu_B B / k_B (T - T^*)$, where T^* is the Curie-Weiss temperature. The sign of T^* indicates the existence of tunable ferromagneticlike ($T^* > 0$) and antiferromagneticlike ($T^* < 0$) coupling in hydrogenated graphene. However, the lack of hysteresis of *MR* or anomalous Hall effect below $|T^*|$ points to the fact that long-range magnetic order did not emerge, which we attribute to the competition of different magnetic orders and disordered arrangement of magnetic moments on graphene. We also find that localized impurity states introduced by H adatoms could modify the capacitance of hydrogenated graphene. This work provides a way to extract information from large negative *MR* behavior and can be a key to understanding interactions of magnetic moments in graphene.

I. INTRODUCTION

Magnetism in graphene induced by nonmagnetic defects has attracted a great deal of attention in recent years [1–15]. From a theoretical point of view, point defects that remove p_z orbitals in π-graphene can create single-electron occupying π states around the missing orbitals, and therefore introduce local magnetic moments in graphene [1–4]. The moments can interact with each other ferromagnetically (antiferromagnetically) when they occupy the same (opposite) graphene lattice [2,3]. Experimentally, such local magnetic moments can be directly imaged and manipulated [4,5] using scanning tunneling microscopy. The moments are characteristic of two spin-split density of states peaks close to the Dirac point, with spatial extension of several nanometers [4,5], suggesting the long-range exchange interaction between the moments can take place [4].

The existence of such local moments and interactions between them naturally leads to the question: what are the electrical transport properties of graphene with magnetic defects and whether there is global magnetic order in graphene with point defects? Since generating local moments on graphene surface in a controlled manner is challenging, magnetotransport of graphene with *in-situ* or *ex-situ* randomly generated carbon vacancy [6,8] or adatoms like hydrogen [11,12], fluorine [9,10,13], or ozone [7] has been studied. Spin-flip scattering [10] and Kondo effect [8] are found in graphene with

point defects, which provides strong evidence that defects in graphene are indeed magnetic and the local moments can strongly couple with conduction electrons [8]. The magnetic moments are also found to scatter pure spin current and generate exchange field in graphene [14]. However, typical behavior of global magnetism like hysteresis loop of magnetoresistance (*MR*) or anomalous Hall effect is not reported. We notice that in the magnetotransport of graphene with local defects [8–11], colossal negative *MR* is widely observed yet not fully understood. These negative *MR* can extend to magnetic field as large as 9 T without saturation, and could be up to -95% [8–11]. The origin of this negative *MR* is not likely to be weak localization (WL) since a typical feature of WL in graphene is within the range of B $\lesssim 0.5$ T and within a magnitude on the order of $\Delta\sigma \sim e^2/h$ [8,10,16–18]. There are proposals that the negative *MR* is caused by strong localization or adatom-induced magnetism [9].

In this work, we report the magnetotransport of *in-situ* hydrogenated graphene in ultrahigh-vacuum (UHV) environment. Similar nonsaturating negative *MR* is observed. We find that for most combinations of electron density (n_e) and H adatom density (n_H), the *MR* curves at different temperature can be scaled to one single trail when they are plotted against $\alpha = \mu_B B / k_B (T - T^*)$, where T^* is the Curie-Weiss temperature. The magnitude and sign of T^* can change systematically with n_e and n_H, indicating tunable ferromagneticlike (FM) or antiferromagneticlike (AFM) coupling. Furthermore, we find that the relationship between T^* and n_H agrees with the theoretically predicted [19] power laws for AFM-like coupling at relatively low carrier density, which provides

*chenjianhao@pku.edu.cn

evidence for validity of the scaling method. At higher carrier density, FM-like coupling appears, instead of theoretically predicted nonmagnetic state [20]. Similar to previous work, the evidence for long-range global order is not observed, which may be due to competition of the FM-like and AFM-like magnetic orders or the disordered arrangement of the local defects in the system. We also find the capacitance of hydrogenated graphene is substantially modified by localized impurity states.

II. EXPERIMENTAL METHODS

The monolayer graphene sample used in this experiment is mechanically exfoliated on 300-nm/500-μm SiO$_2$/Si substrates using Scotch tape. Its thickness is decided with AFM together with optical color code and subsequently confirmed by the half-integer quantum Hall effect [21]. The quality of the pristine sample is also checked by Raman spectroscopy (see figure S3 in Supplemental Material [22]). Graphene device is fabricated using standard electron-beam lithography (EBL) technique and metal contact of Cr 5 nm/Au 50 nm. The device is etched into Hall-bar geometry using reactive ion etching. The etching process is done with 100-sccm O$_2$ at 100-W power for 30 s. Magnetotransport measurement is done in our home-built *in-situ* transport system, with ultrahigh-vacuum environment (up to 10^{-9} Torr) to substantially reduce impurity absorption on sample surface between each round of hydrogen doping. The sample temperature of the measurement ranges from 5.8 to 62 K, since we found that higher temperature may cause desorption of H atoms from the graphene surface. The applied magnetic field is perpendicular to the graphene sample and the maximum field is 9 T. The graphene is doped using hydrogen atom source, which generates hydrogen atoms with radio-frequency (rf) plasma (13.56 MHz). The amount of hydrogen atoms is controlled by the rf power and doping time. The hydrogen plasma is usually generated at a vacuum of 10^{-2} Torr and at rf power of 60 W. Time of each round of doping varies from 5 to 10 s, controlled with a mechanical shutter. Hydrogen ions are also generated in the process and are deflected with horizontal electrical field to avoid hitting the graphene surface and generating vacancy defects in graphene (schematics of the experimental setup can be found in figure S1 of Supplemental Material [22]). Transport measurement is done using low-frequency lock-in amplifier technique. All the carrier density, unless specified, is calculated using parallel capacitor model $n_e = C_g(V_g - V_D)$, where V_g is gate voltage, V_D is Dirac point location, and C_g for 300 nm SiO$_2$ is 7.2×10^{10} cm^{-2} V^{-1}.

III. RESULTS AND DISCUSSION

in-situ experiments allow us to explore the effect of adatom doping on the transport properties of the sample in an almost continuous way. That means we can start from a pristine sample and give it a small amount of doping, which can be controlled by the doping power and doping time. Then we can stop and do thorough magnetotransport measurement after each round of doping. Usually the doping and measuring procedure will be repeated for 5 to 20 times, depending on the amount of hydrogen at each round of doping and on the final
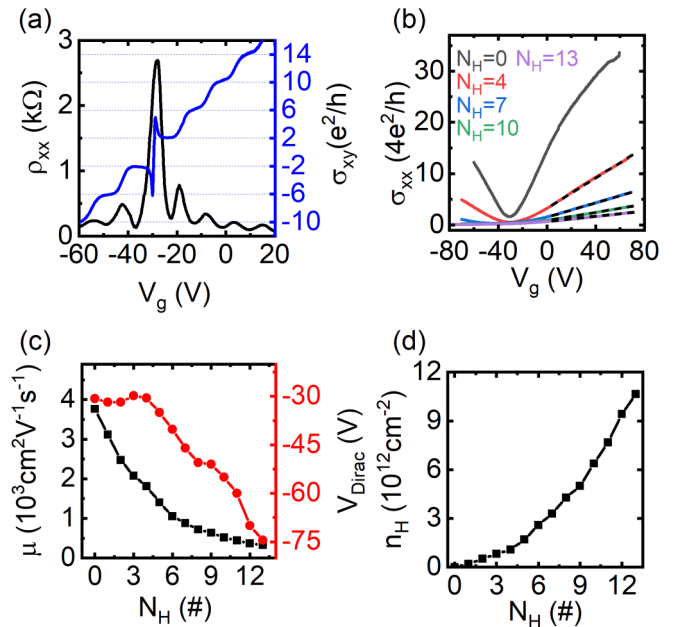

FIG. 1. Transport property of pristine and hydrogenated graphene. (a) Quantum Hall effect of pristine graphene at $T = 5.8$ K, $B = 9$ T. (b) Conductivity of graphene after hydrogenation at $T = 5.8$ K. $N_H = 0, 1, 2, \dots$ means hydrogenation round, $N_H = 0$ corresponds to pristine graphene. Dashed lines are straight lines as guide for the eye. (c) Mobility at $T = 5.8$ K and Dirac point shift of hydrogenated graphene. (d) Estimated hydrogen adatom density on graphene after each round of hydrogenation.

device quality. In the end, we obtain a curve of transport property versus the amount of doping. In this process, the sample is in UHV for most of the time (except during doping when the hydrogen partial pressure will increase to $\sim$10^{-2} Torr), so it is hardly influenced by unwanted impurity absorption from the environment.

In our graphene *in-situ* hydrogenation experiment, the as-fabricated device is of good quality, which is manifested by the well-developed quantum Hall effect, as shown in Fig. 1(a). Note that the initial Dirac point of the device is away from zero, which might be a result of initial surface absorbates as the sample surface is exposed for *in-situ* doping. Nonetheless, this initial offset will not affect the physics probed in this experiment since the key data are the difference during each round of *in-situ* treatment. If needed, such offset could be removed by using hBN substrate [23] or using Hexam-ethyldisilazane (HMDS)-treated SiO$_2$ surface [24]. After each round of hydrogenation, the sample still shows typical V-shaped conductivity vs V_g curves [Fig. 1(b)], with the mobility reduced [Fig. 1(c)], as expected for increasing disorder in the system. The Dirac point shifts to negative gate voltages [Fig. 1(c)], which means that hydrogen atoms bring extra electron doping to graphene, consistent with previous Angle Resolved Photoemission Spectroscopy (ARPES) study [25]. We notice that σ_{xx} is proportional to V_g, thus the carrier density $n \sim C_g(V_g - V_D)$, when the Fermi surface is far from the Dirac point [as indicated by dashed lines in Fig. 1(b)], which is a typical result of charged impurity scattering [26] and defect scattering [6]. For graphene with screened charged impurity
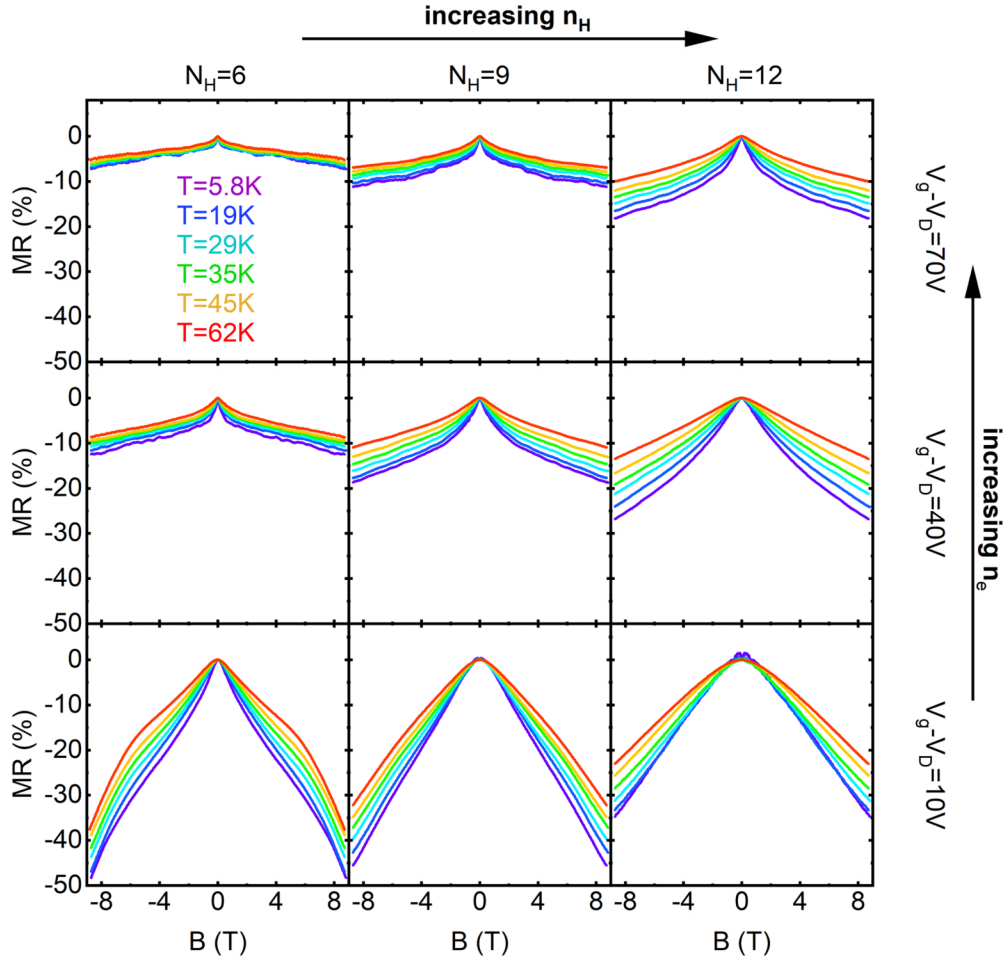
FIG. 2. Magnetoresistance of hydrogenated graphene at different hydrogen density (n_H) and electron density (n_e). All plots use the same scale for comparison. N_H means hydrogenation round. Different color stands for different temperatures. Zoom-in of *MR* for the ±0.5-T range can be found in figure S7 of Supplemental Material [22].

[26] or midgap states [6], we have $\sigma_{xx} = C(e^2/h)(|n|/n_{imp})$, where C is a constant depending on the details of impurity, n is the carrier density in graphene, and n_{imp} is the impurity density. A hydrogen atom chemisorbed on graphene essentially changes the original sp^2 hybridization of the carbon atom to sp^3 and remove the p_z orbital [4,27]. In this sense, H chemisorption is equivalent to creation of carbon vacancy on graphene. For the latter case, previous work [6] gives the value of C to be about 4. Here, we use the same value as an estimate for the order of magnitude. Figure 1(d) shows the estimated hydrogen density on graphene. Maximum hydrogen density is on the order of 10^{13} cm^{-2}, which gives a maximum doping coverage of 0.28% and an average H atom distance down to 2.1 nm.

Since the Dirac point is far from zero after several rounds of H doping, we focus on the magneto-transport on the electron side. The *MR* behavior of the hole side is similar to that of the electron side and can be found in figure S8 of Supplemental Material [22]. Figure 2 shows the *MR* of hydrogenated graphene at different combinations of electron density (n_e) and hydrogen density (n_H). We find for most cases the *MR* is negative. The negative *MR* is not saturating up to 9 T, and the maximum value can be −52%. The negative *MR* is found to decay with increasing temperature. Similar

negative *MR* has already been observed in graphene with carbon vacancy [8] and fluorine adatoms [9,10]. We have repeated *in-situ* hydrogenation experiment on multiple graphene devices and similar behavior is found (see figures S14 and S15 of Supplemental Material [22]).

There are multiple possible origins of such *MR* behavior. In the small-field regime ($B < 0.5$ T), the *MR* is confirmed to originate from weak localization [8] or weak antilocalization, which we will discuss in detail elsewhere. The highly interesting *MR* in the large-field regime will be discussed in this paper. At the first five rounds (see figure S6 of Supplemental Material [22]) of hydrogenation, Shubnikov–de Haas (SdH) oscillations clearly exist, contributing to some *MR* features. Note that SdH oscillation can give mobility and Hall density at high magnetic fields [28]; the difference with low-field properties can give crucial information on the scattering source in graphene, which will be interesting to study in future experiments (for preliminary data see figure S13 of Supplemental Material [22]). For negative *MR* not affected by SdH oscillations (e.g., with higher impurity density and lower carrier mobility), there are proposals [9] that the phenomenon can be caused by strong localization [29,30] or adatom-induced magnetism [10]. The strong localization model suggests that the graphene is divided into disconnected conducting areas,

and at finite temperature, charge carriers can hop from one area to another. In this regime, the graphene resistivity should be described by the variable-range hopping (VRH) model [29,31]. We analyzed the relationship of resistance and temperature of our hydrogenated graphene, and found that it does not follow either Efros-Shklovskii (ES)-type or Mott-type VRH model [29,31] (see figure S9 of Supplemental Material [22]). Even for the resistance at the Dirac point, we find that $\ln(R_{\text{Dirac}})$ is not proportional to T^{-1}, $T^{-1/2}$, or $T^{-1/3}$, which further rules out a strong thermal activation effect or variable-range hopping effect [32]. In fact the localization is relatively weak even for the high H density samples (see figures S9b and 9d of Supplemental Material [22]). Therefore, strong localization can be ruled out for our experiment and the negative *MR* can only be caused by the magnetic moments on graphene.

Negative *MR* in magnetic materials is quite common, like diluted magnetic semiconductors [33–36], alloys [37–39], as well as oxides [40,41]. However, the magnitude and functional form of the negative *MR* in hydrogenate graphene (similarly in graphene with atomic vacancy [8] and fluorine [9,10]) is difficult to fit directly to existing theories [9]. Nonetheless, negative *MR* in magnetic materials usually originates from charge carriers scattered by the isolated magnetic moments, which is a function of $MR \equiv MR(M, \alpha)$ [33,41], where M is the total magnetization of the material and $\alpha \equiv \mu_B B/k_B(T - T^*)$. Here T^* is the Curie-Weiss temperature, describing the exchange effect between the magnetic moments. If the material is paramagnetic or above its critical temperature, we can write the low-field magnetization as $M = \chi H \propto H/k_B(T - T^*) = M(\alpha)$. Thus we can express *MR* as a function of α, e.g., $MR = MR(\alpha)$ before magnetic ordering occurs.

Important information can be readily extracted from the fact that $MR = MR(\alpha)$, without going into the detailed functional form of *MR*, which could depend on material-specific parameters. Since there is no explicit dependence on T in $MR(\alpha)$ curves, for a certain combination of n_e and n_H, the form of *MR* should be invariant at different temperatures when plotted against $\alpha \equiv \mu_B B/k_B(T - T^*)$. In other words, *MR* for any specific n_e and n_H at all T above magnetic ordering temperature can be scaled into one single trail when we plot *MR* vs α, if we used the right T^*. For example, in Fig. 3(a), we plot *MR* curves vs α for three different trial values of T^* for the 12th hydrogenation round and at electron density $V_g - V_D = 40$ V. Only data corresponding to temperature higher than 25 K and magnetic field lower than 3 T [13] are used to fulfill the aforementioned criteria. As we can see, the curves can perfectly collapse at $T^* = -7.2$ K. Mathematically, T^* is obtained by minimizing the square sum $S = \sum (MR_i - \overline{MR})^2$; detailed description can be found in figure S10 in Supplemental Material [22]. Repeating that procedure for other n_e and n_H gives a two-dimensional plot of T^* as shown in Fig. 3(b), which reveals the phase diagram of the effective coupling type and strength for the magnetic moments in hydrogenated graphene. Since the sign of the Curie-Weiss temperature T^* indicates the type of magnetic coupling, we can clearly find that the phase diagram in Fig. 3(b) is divided into ferromagneticlike ($T^* > 0$) regime and antiferromagneticlike ($T^* < 0$) regime.
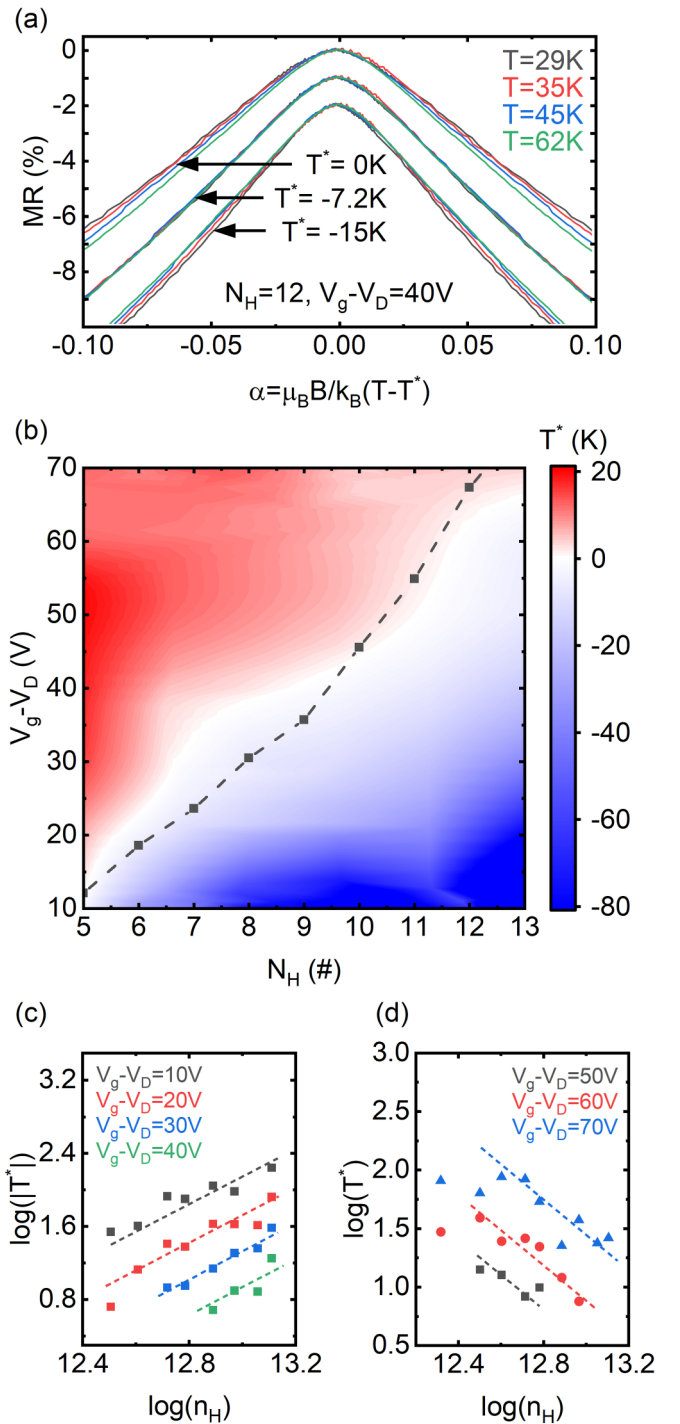

FIG. 3. Scaling and magnetic phase diagram of hydrogenated graphene. (a) Scaling of *MR* for $N_H = 12$, $V_{g-}V_D = 40$ V. N_H means hydrogenation round. (b) Phase diagram of scaled Curie-Weiss temperature T^*. Dashed line corresponds to $n_e/n_H \simeq 3.1$. (c) $|T^*|$ vs hydrogen density n_H in the AFM-like regime in (b), in log-log scale. Dashed lines are $|T^*| \propto n_H^{3/2}$, as guide for the eye. (d) T^* vs n_H in the FM-like regime in (b), in log-log scale. Dashed lines are $T^* \propto n_H^{-3/2}$, as guide for the eye.

Previous theoretical work [19,20,42] predicted that AFM order can exist in dilute doped graphene at low carrier density, if the magnetic moments are evenly distributed on both sublattices. In this case, $|T^*|$ is predicted to be proportional to $n_H^{\gamma/2}$,

where γ is the decaying index of Ruderman-Kittel-Kasuya-Yosida (RKKY) interaction $J(r) \propto 1/r^{\gamma}$. In graphene, the value of γ is found to be 3, due to the absence of extended Fermi surface [19,20]. We take $|T^*|$ under various electron densities and plot them against n_H in log-log scale, as shown in Fig. 3(c). We find $|T^*| \propto n_H^{3/2}$ can perfectly fit our scaling data points, which proves the validity of our scaling method.

At higher carrier density, the RKKY interaction will develop Friedel oscillations [20,43]. It would give a random sign to the exchange interaction of the magnetic moments with distance larger than $r > 1/\sqrt{n_e}$. So, ordered magnetic phase is expected to be suppressed at a sufficiently large n_e/n_H ratio [20]. In our phase diagram, $|T^*|$ of AFM order is indeed dropping with increasing carrier concentration and the boundary of AFM order is close to a line corresponding to $n_e/n_H \simeq 3.1$, as depicted by the dashed line in Fig. 3(b). However, over this boundary, $T^* > 0$, indicating that FM-like magnetic coupling appears, different from the predicted nonmagnetic state [20] or competition between AFM and Kondo effect [44]. We also plot T^* vs n_H in this regime in Fig. 3(d) using log-log scale, and surprisingly find the relationship $T^* \propto n_H^{-3/2}$ can describe our scaling data quite well. We notice this fits the theoretical prediction for the case that magnetic moments are only on one set of graphene sublattices [45]. Even though our experimental condition is definitely different from the premise of Ref. [45], the surprising agreement might indicate the emergence of FM-like coupling and it might point to something deeper than a mere coincidence. Since at large n_e the effective length of exchange interaction is small [20,43], our experimental finding might point to a locally ferromagnetically coupled configuration of the magnetic moments on graphene. Clearly, more theoretical work is required to understand this observation.

Another point to note is the relation between magnetic ordering temperature T_N (T_c) and the Curie-Weiss temperature T^*. Here the Curie-Weiss temperature T^* is not the temperature where magnetic order appears, but rather a measure of type (the sign of T^*) and strength (the magnitude of T^*) of magnetic coupling of local moments on graphene. In the AFM-like regime, $|T^*|$ can be higher than 80 K; in the FM-like regime, T^* can reach about 20 K. But, no evidence of long-range FM order, such as hysteresis loop in MR and R_{xy}, is observed when $T < T^*$ in the FM-like regime. So, the actual ordering temperature T_N (T_c) must be much lower than the Curie-Weiss temperature. A possible explanation could be that the long-ranged order is suppressed by the competition between FM and AFM order; another possibility arises from the disordered location of the magnetic moments in the system. Indeed, in spin liquid or systems with magnetic frustration [46,47], the actual critical (ordering) temperature can be 5 to 10 times smaller than the Curie-Weiss temperature. Future work at lower temperature will help to clarify this issue.

Finally, we report our finding on the Hall density of states of hydrogenated graphene. Figure 4(a) shows the Hall resistance of pristine and hydrogenated graphene. There is no sign of anomalous Hall effect after hydrogenation, but the slope of the Hall resistance is modified. Figure 4(b) shows the measured Hall carrier density and linear fits of $n = C_H(V_g - V_D)$, where C_H stands for the capacitance calculated from Hall-effect carrier density. The left axis of Fig. 4(c) shows the
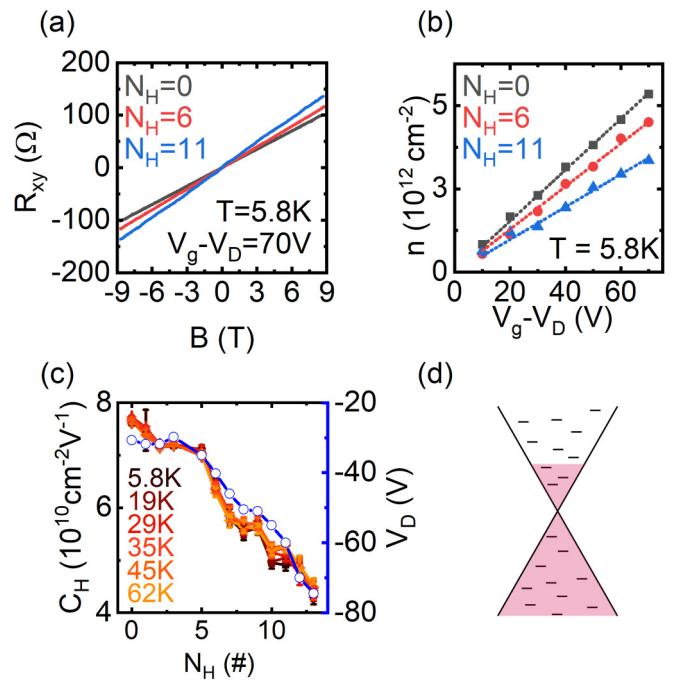

FIG. 4. Density of states in hydrogenated graphene. (a) Hall resistance of pristine and hydrogenated graphene. (b) Dependence of Hall carrier density on gate voltage. Dashed lines are linear fits to $n = C_H(V_g - V_D)$. (c) Solid dots: capacitance at various temperatures calculated from Hall carrier density. Open circle: Dirac point position. (d) Illustration of hydrogenated graphene band structure. Short dash stands for energy levels of localized impurity states.

fitted capacitance C_H as a function of the hydrogenation round N_H and at different temperatures from 5.8 to 62 K. Before hydrogenation, C_H (7.9×10^{10} cm^{-2} V^{-1}) is a little higher than the value of 300-nm SiO$_2$ dielectric parallel capacitor C_g (7.2×10^{10} cm^{-2} V^{-1}) [48], so we expect the Hall mobility to be slightly higher than the Drude mobility [49,50]. We find that C_H drops almost 50% after hydrogenation and it is almost temperature independent.

The origin of the modification of C_H can be understood as the following: First of all, hydrogen atoms would do very little in changing the dielectric constant of the 300-nm SiO$_2$ substrate, especially for the portion of the SiO$_2$ under the protection of the graphene flake. Thus it is not a changing dielectric constant that is responsible for the change in C_H. Second, the change in Hall resistance slopes cannot be related to magnetic ordering in the sample, otherwise, the Hall signal should depend on temperature prominently, similar to behavior of the longitudinal MR. One possible reason is the localized impurity states due to hydrogenation. Previous work pointed out that there will be impurity states around the Fermi level for graphene with vacancy defects [51] or H adatom impurity [52]. And, the impurity states are found to be quasilocalized [51–53], such that a moderate change in temperature (from 5.8 to 62 K) will not cause delocalization [54], and the only way to deplete such localized electron would be by the change of Fermi level via V_g. These localized states will reduce the carrier density that can be observed in transport, leading to a reduction in C_H. The physical picture of

such localized states is illustrated in Fig. 4(d). Furthermore, if we plot the shift of the Dirac point together with the change in C_H, as shown in the right axis of Fig. 4(c), we find that the two curves almost collapse. Since one hydrogen adatom provides a fixed doping to the sample, therefore the amount of impurity states created by hydrogen absorption should be reflected by a proportional shift in the Dirac point in graphene, which is consistent with the physical picture illustrated in Fig. 4(d).

IV. CONCLUSION

In summary, we studied the magnetotransport of hydrogenated graphene with *in-situ* doping method. We find that hydrogenated graphene shows large negative *MR*, similar to graphene with carbon vacancy [8] and fluorine adatoms [9,10]. By scaling the *MR* curves using proper Curie-Weiss temperatures, two different regimes are found with FM-like and AFM-like magnetic coupling, respectively. The type of magnetic coupling is jointly tunable by carrier density and hydrogen density, and there is no evidence of long-ranged mag-

netic ordering. The existence of AFM-like coupling is a result of RKKY interaction of H adatom induced magnetic moments on graphene. But, the appearance of FM-like coupling is unexpected, which requires more theoretical investigation. Finally, we found that hydrogen adatom induced localized impurity states has a substantial impact in the charge-carrier density of states. This work provides a method to extract key information from large negative *MR* in similar physical systems and could be a key factor to better understand 2D magnetism.

[1] M. A. H. Vozmediano, M. P. López-Sancho, T. Stauber, and F. Guinea, Local defects and ferromagnetism in graphene layers, Phys. Rev. B **72**, 155121 (2005).

[2] O. V. Yazyev, Magnetism in Disordered Graphene and Irradiated Graphite, Phys. Rev. Lett. **101**, 037203 (2008).

[3] D. Soriano, N. Leconte, P. Ordejón, J.-C. Charlier, J.-J. Palacios, and S. Roche, Magnetoresistance and Magnetic Ordering Fingerprints in Hydrogenated Graphene, Phys. Rev. Lett. **107**, 016602 (2011).

[4] H. González-Herrero, J. M. Gómez-Rodríguez, P. Mallet, M. Moaied, J. J. Palacios, C. Salgado, M. M. Ugeda, J.-Y. Veuillen, F. Yndurain, and I. Brihuega, Atomic-scale control of graphene magnetism by using hydrogen atoms, Science **352**, 437 (2016).

[5] Y. Zhang, S.-Y. Li, H. Huang, W.-T. Li, J.-B. Qiao, W.-X. Wang, L.-J. Yin, K.-K. Bai, W. Duan, and L. He, Scanning Tunneling Microscopy of the π Magnetism of a Single Carbon Vacancy in Graphene, Phys. Rev. Lett. **117**, 166801 (2016).

[6] J.-H. Chen, W. G. Cullen, C. Jang, M. S. Fuhrer, and E. D. Williams, Defect Scattering in Graphene, Phys. Rev. Lett. **102**, 236805 (2009).

[7] J. Moser, H. Tao, S. Roche, F. Alzina, C. M. Sotomayor Torres, and A. Bachtold, Magnetotransport in disordered graphene exposed to ozone: From weak to strong localization, Phys. Rev. B **81**, 205445 (2010).

[8] J.-H. Chen, L. Li, W. G. Cullen, E. D. Williams, and M. S. Fuhrer, Tunable Kondo effect in graphene with defects, Nat. Phys. **7**, 535 (2011).

[9] X. Hong, S. H. Cheng, C. Herding, and J. Zhu, Colossal negative magnetoresistance in dilute fluorinated graphene, Phys. Rev. B **83**, 085410 (2011).

[10] X. Hong, K. Zou, B. Wang, S. H. Cheng, and J. Zhu, Evidence for Spin-Flip Scattering and Local Moments in Dilute Fluorinated Graphene, Phys. Rev. Lett. **108**, 226602 (2012).

[11] B. R. Matis, F. A. Bulat, A. L. Friedman, B. H. Houston, and J. W. Baldwin, Giant negative magnetoresistance and a transition from strong to weak localization in hydrogenated graphene, Phys. Rev. B **85**, 195437 (2012).

[12] J. Balakrishnan, G. K. W. Koon, M. Jaiswal, A. C. Neto, and B. Özyilmaz, Colossal enhancement of spin-orbit coupling in weakly hydrogenated graphene, Nat. Phys. **9**, 284 (2013).

[13] R. R. Nair, M. Sepioni, I. L. Tsai, O. Lehtinen, J. Keinonen, A. V. Krasheninnikov, T. Thomson, A. K. Geim, and I. V. Grigorieva, Spin-half paramagnetism in graphene induced by point defects, Nat. Phys. **8**, 199 (2012).

[14] K. M. McCreary, A. G. Swartz, W. Han, J. Fabian, and R. K. Kawakami, Magnetic Moment Formation in Graphene Detected by Scattering of Pure Spin Currents, Phys. Rev. Lett. **109**, 186604 (2012).

[15] C.-Y. Cai and J.-H. Chen, Electronic transport properties of Co cluster-decorated graphene, Chin. Phys. B **27**, 67304 (2018).

[16] U. Chandni, E. A. Henriksen, and J. P. Eisenstein, Transport in indium-decorated graphene, Phys. Rev. B **91**, 245402 (2015).

[17] J. A. Elias and E. A. Henriksen, Electronic transport and scattering times in tungsten-decorated graphene, Phys. Rev. B **95**, 075405 (2017).

[18] S. V. Morozov, K. S. Novoselov, M. I. Katsnelson, F. Schedin, L. A. Ponomarenko, D. Jiang, and A. K. Geim, Strong Suppression of Weak Localization in Graphene, Phys. Rev. Lett. **97**, 016801 (2006).

[19] T. Fabritius, N. Laflorencie, and S. Wessel, Finite-temperature ordering of dilute graphene antiferromagnets, Phys. Rev. B **82**, 035402 (2010).

[20] V. V. Cheianov, O. Syljuåsen, B. L. Altshuler, and V. Fal'ko, Ordered states of adatoms on graphene, Phys. Rev. B **80**, 233409 (2009).

[21] K. S. Novoselov, E. McCann, S. V. Morozov, V. I. Fal'ko, M. I. Katsnelson, U. Zeitler, D. Jiang, F. Schedin, and A. K. Geim, Unconventional quantum hall effect and Berry's phase of 2π in bilayer graphene, Nat. Phys. **2**, 177 (2006).

[22] See Supplemental Material at http://link.aps.org/supplemental/10.1103/PhysRevB.102.045402 for the details of experiment setup, sample quality characterization, hole-side *MR* behavior, high-field data, and similar results from a second sample.

[23] C. R. Dean, A. F. Young, I. Meric, C. Lee, L. Wang, S. Sorgenfrei, K. Watanabe, T. Taniguchi, P. Kim, K. L. Shepard,

and J. Hone, Boron nitride substrates for high-quality graphene electronics, Nat. Nanotechnol. **5**, 722 (2010).

[24] J. M. Caridad, S. R. Power, M. R. Lotz, A. A. Shylau, J. D. Thomsen, L. Gammelgaard, T. J. Booth, A.-P. Jauho, and P. Bøggild, Conductance quantization suppression in the quantum hall regime, Nat. Commun. **9**, 659 (2018).

[25] R. Balog, B. Jørgensen, L. Nilsson, M. Andersen, E. Rienks, M. Bianchi, M. Fanetti, E. Lægsgaard, A. Baraldi, S. Lizzit, Z. Sljivancanin, F. Besenbacher, B. Hammer, T. G. Pedersen, P. Hofmann, and L. Hornekær, Bandgap opening in graphene induced by patterned hydrogen adsorption, Nat. Mater. **9**, 315 (2010).

[26] S. Adam, E. H. Hwang, V. M. Galitski, and S. Das Sarma, A self-consistent theory for graphene transport, Proc. Natl. Acad. Sci. USA **104**, 18392 (2007).

[27] J. O. Sofo, G. Usaj, P. S. Cornaglia, A. M. Suarez, A. D. Hernández-Nieves, and C. A. Balseiro, Magnetic structure of hydrogen-induced defects on graphene, Phys. Rev. B **85**, 115405 (2012).

[28] E. Diez, Y. P. Chen, S. Avesque, M. Hilke, E. Peled, D. Shahar, J. M. Cerveró, D. L. Sivco, and A. Y. Cho, Two-dimensional electron gas in InGaAs/InAlAs quantum wells, Appl. Phys. Lett. **88**, 052107 (2006).

[29] H. W. Jiang, C. E. Johnson, and K. L. Wang, Giant negative magnetoresistance of a degenerate two-dimensional electron gas in the variable-range-hopping regime, Phys. Rev. B **46**, 12830 (1992).

[30] H. Gu, J. Guo, R. Sadu, Y. Huang, N. Haldolaarachchige, D. Chen, D. P. Young, S. Wei, and Z. Guo, Separating positive and negative magnetoresistance for polyaniline-silicon nanocomposites in variable range hopping regime, Appl. Phys. Lett. **102**, 212403 (2013).

[31] K. Bennaceur, P. Jacques, F. Portier, P. Roche, and D. C. Glattli, Unveiling quantum hall transport by Efros-Shklovskii to Mott variable-range hopping transition in graphene, Phys. Rev. B **86**, 085433 (2012).

[32] C. Cobaleda, S. Pezzini, E. Diez, and V. Bellani, Temperature- and density-dependent transport regimes in a h-BN/bilayer graphene/h-BN heterostructure, Phys. Rev. B **89**, 121404 (2014).

[33] M. Csontos, T. Wojtowicz, X. Liu, M. Dobrowolska, B. Jankó, J. K. Furdyna, and G. Mihály, Magnetic Scattering of Spin Polarized Carriers in (In,Mn)Sb Dilute Magnetic Semiconductor, Phys. Rev. Lett. **95**, 227203 (2005).

[34] T. Dietl, Interplay between carrier localization and magnetism in diluted magnetic and ferromagnetic semiconductors, J. Phys. Soc. Jpn. **77**, 031005 (2008).

[35] T. Dietl, H. Ohno, and F. Matsukura, Hole-mediated ferromagnetism in tetrahedrally coordinated semiconductors, Phys. Rev. B **63**, 195205 (2001).

[36] C. Haas, Spin-disorder scattering and magnetoresistance of magnetic semiconductors, Phys. Rev. **168**, 531 (1968).

[37] M.-T. Béal-Monod and R. Weiner, Negative magnetoresistivity in dilute alloys, Phys. Rev. **170**, 552 (1968).

[38] F. T. Hedgcock, W. B. Muir, T. W. Raudorf, and R. Szmidt, Magnetoresistance and Magnetization in Cu: Fe Alloys Below 4.2k, Phys. Rev. Lett. **20**, 457 (1968).

[39] R. More and H. Suhl, Magnetoresistance of Dilute Magnetic Alloys, Phys. Rev. Lett. **20**, 500 (1968).

[40] M. F. Hundley, M. Hawley, R. H. Heffner, Q. X. Jia, J. J. Neumeier, J. Tesmer, J. D. Thompson, and X. D. Wu, Transport-magnetism correlations in the ferromagnetic oxide $La_{0.7}Ca_{0.3}MnO_3$, Appl. Phys. Lett. **67**, 860 (1995).

[41] A. Brinkman, M. Huijben, M. van Zalk, J. Huijben, U. Zeitler, J. C. Maan, W. G. van der Wiel, G. Rijnders, D. H. A. Blank, and H. Hilgenkamp, Magnetic effects at the interface between non-magnetic oxides, Nat. Mater. **6**, 493 (2007).

[42] J. J. Palacios, J. Fernández-Rossier, and L. Brey, Vacancy-induced magnetism in graphene and graphene ribbons, Phys. Rev. B **77**, 195428 (2008).

[43] L. Brey, H. A. Fertig, and S. Das Sarma, Diluted Graphene Antiferromagnet, Phys. Rev. Lett. **99**, 116802 (2007).

[44] A. Allerdt, A. E. Feiguin, and S. Das Sarma, Competition between Kondo effect and RKKY physics in graphene magnetism, Phys. Rev. B **95**, 104402 (2017).

[45] K. Szałowski, Critical temperature of two-dimensional hydrogenated multilayer graphene-based diluted ferromagnet, Carbon **108**, 327 (2016).

[46] L. Balents, Spin liquids in frustrated magnets, Nature (London) **464**, 199 (2010).

[47] A. Ramirez, Strongly geometrically frustrated magnets, Ann. Rev. Mater. Sci. **24**, 453 (1994).

[48] Y. Zhang, Z. Jiang, J. Small, M. Purewal, Y.-W. Tan, M. Fazlollahi, J. Chudow, J. Jaszczak, H. Stormer, and P. Kim, Landau-Level Splitting in Graphene in High Magnetic Fields, Phys. Rev. Lett. **96**, 136806 (2006).

[49] S. Kim, J. Nah, I. Jo, D. Shahrjerdi, L. Colombo, Z. Yao, E. Tutuc, and S. K. Banerjee, Realization of a high mobility dual-gated graphene field-effect transistor with Al_2O_3 dielectric, Appl. Phys. Lett. **94**, 062107 (2009).

[50] S. Pezzini, C. Cobaleda, E. Diez, and V. Bellani, Quantum interference corrections to magnetoconductivity in graphene, Phys. Rev. B **85**, 165451 (2012).

[51] V. M. Pereira, F. Guinea, J. M. B. Lopes dos Santos, N. M. R. Peres, and A. H. Castro Neto, Disorder Induced Localized States in Graphene, Phys. Rev. Lett. **96**, 036801 (2006).

[52] T. O. Wehling, S. Yuan, A. I. Lichtenstein, A. K. Geim, and M. I. Katsnelson, Resonant Scattering by Realistic Impurities in Graphene, Phys. Rev. Lett. **105**, 056802 (2010).

[53] V. M. Pereira, J. M. B. Lopes dos Santos, and A. H. Castro Neto, Modeling disorder in graphene, Phys. Rev. B **77**, 115109 (2008).

[54] V. G. Miranda, L. G. G. V. Dias da Silva, and C. H. Lewenkopf, Coulomb charging energy of vacancy-induced states in graphene, Phys. Rev. B **94**, 075114 (2016).